Crystal Structure at 2.0 Å Resolution of Phosphoribosyl Anthranilate Isomerase from the Hyperthermophile *Thermotoga maritima*: Possible Determinants of Protein Stability[†,#]

Michael Hennig,*[,‡,§] Reinhard Sterner,[||] Kasper Kirschner,[||] and Johan N. Jansonius[‡]

Departments of Structural Biology and Biophysical Chemistry, Biozentrum, University of Basel, Klingelbergstrasse 70, CH-4056 Basel, Switzerland

Received October 30, 1996; Revised Manuscript Received March 3, 1997[⊗]

ABSTRACT: The structural basis of thermostability of proteins is of great scientific and biotechnological interest. Differences in the X-ray structues of orthologous proteins from hyperthermophilic and mesophilic organisms can indicate crucial stabilizing interactions. To this end the crystal structure of dimeric phosphoribosyl anthranilate isomerase from the hyperthermophile *Thermotoga maritima* (tPRAI) was determined using phases derived from the isomorphous replacement method and was refined at 2.0 Å resolution. The comparison to the known 2.0 Å structure of PRAI from *Escherichia coli* (ePRAI) shows that tPRAI has the complete TIM- or $(\beta\alpha)_8$-barrel fold, whereas helix α5 in ePRAI is replaced by a loop. The subunits of tPRAI associate via the N-terminal faces of their central β-barrels. Two long, symmetry-related loops that protrude reciprocally into cavities of the other subunit provide for multiple hydrophobic interactions. Moreover, the side chains of the N-terminal methionines and the C-terminal leucines of both subunits are immobilized in a hydrophobic cluster, and the number of salt bridges is increased in tPRAI. These features appear to be mainly responsible for the high thermostability of tPRAI. In contrast to other hyperthermostable enzymes, tPRAI at 25 °C is catalytically more efficient than ePRAI, mainly due to its small K_M value for the substrate [Sterner, R., Kleemann, G. R., Szadkowski, H., Lustig, A., Hennig, M., & Kirschner, K. (1996) *Protein Sci. 5*, 2000−2008]. The increased number of hydrogen bonds between the phosphate ion and tPRAI compared to ePRAI could be responsible for this effect.

The structural basis of extreme protein thermostability is a highly relevant, but complex and still poorly understood problem. Proteins from hyperthermophilic microorganisms, i.e., those that grow optimally above 80 °C (Adams, 1993; Stetter et al., 1990), offer a unique opportunity to address this question. Comparisons of highly resolved X-ray structures of enzymes with the same fold and function in mesophiles and hyperthermophiles have revealed a number of potentially stabilizing features. In general, thermostable proteins show an increased number of salt bridges or hydrogen bonds (Day et al., 1992; Davies et al., 1993; Kelly et al., 1993; Korndörfer et al., 1995; Yip et al., 1995; Hennig et al., 1995; Tanner et al., 1996; Knegtel et al., 1996, Macedo-Ribeiro et al., 1996), optimized stabilization of α-helices (Kelly et al., 1993; Russell et al., 1994; Hennig et al., 1995), decreased solvent-exposed surface areas (Chan et al., 1995), reduced loop sizes and stabilization of turns (Russell et al., 1994), and fixation of the N- and C- terminus (Day et al., 1992; Hennig et al., 1995; Macedo-Ribeiro et al., 1996) as well as improved intermolecular hydrophobic interactions within oligomers (Imada et al., 1991; Fujinaga et al., 1993; Russell et al., 1994; Delboni et al., 1995).

The hyperthermophile *Thermotoga maritima* was isolated from geothermally heated locales on sea floors and has a maximum growth temperature of 90 °C (Huber et al., 1986). In *Escherichia coli*, e*trp*C(F) encodes a bifunctional enzyme that catalyzes the fourth and fifth steps in tryptophan biosynthesis. Each catalytic activity is sustained by a distinct domain having the triose phosphate isomerase (TIM)-[1] or $(\beta\alpha)_8$-barrel fold (Priestle et al., 1987; Banner et al., 1975; Reardon & Farber, 1995). Expression of the truncated e*trp*F gene yields a fully active, monomeric phosphoribosyl anthranilate isomerase (ePRAI; Eberhard, et al., 1995). Recently, the *trp*F gene of *T. maritima* (t*trp*F) was cloned, sequenced, and expressed heterologously in *E. coli* (Sterner et al., 1995, 1996). tPRAI, the gene product of t*trp*F, is an extremely thermostable homodimer.

Here the X-ray structure of tPRAI is presented at a resolution of 2.0 Å. In accordance with solution studies, tPRAI crystallizes as a homodimer. The subunits have a canonical $(\beta\alpha)_8$-barrel topology and are associated primarily via the N-terminal faces of their central β-barrels through multiple hydrophobic interactions. This "back to back

[†] This work was supported by grants from the Swiss National Science Foundation to J.N.J. (31-36432.92) and to K.K. (31-32369.91).

[#] The coordinates for tPRAI have been deposited with the Brookhaven Protein Data Bank (entry code 1NSJ).

* Author to whom correspondence should be addressed: phone, +41 61 6886046; fax, +41 61 6887408; email, Michael.Hennig@roche.com.

[‡] Department of Structural Biology.

[§] Current address: F. Hoffmann-La Roche AG, Pharma Research PRPI-S 65/308, CH-4070 Basel, Switzerland.

[||] Department of Biophysical Chemistry.

[⊗] Abstract published in *Advance ACS Abstracts,* April 15, 1997.

[1] Abbreviations: tPRAI, phosphoribosyl anthranilate isomerase from *Thermotoga maritima*; ePRAI, phosphoribosyl anthranilate isomerase from *Escherichia coli*; TIM, triose phosphate isomerase; eIGPS and sIGPS, indole-3-glycerol phosphate synthases from *E. coli* and *Sulfolobus solfataricus*, respectively; eIGPS:PRAI, bifunctional indole-3-glycerol phosphate synthase and phosphoribosyl anthranilate isomerase from *E. coli*; PRA, phosphoribosyl anthranilate; EMTS, ethylmercury thiosalicylate.

S0006-2960(96)02718-3 CCC: $14.00

Table 1: Data Collection Statistics for Native and Derivative Crystals of tPRAI[a]

	max resolution (Å)	total reflections	unique reflections	completeness (%)	R_{sym}[b] (%)	R_{iso}[c] (%)	binding sites	R_c[d] (%)	phasing power
native	2.0	118 018	17 903	98.8	6.4				
$Hg(CH_3COO)_2$	2.8	17 981	6 873	99.7	6.3	14.8	Cys7, Cys91	59.0	1.1
EMTS	4.0	9 999	2 500	99.1	6.7	22.1	Cys7, Cys91	80.0	0.6

[a] Derivatives were prepared by soaking the crystals in a solution of 100 mM MES buffer containing 2.0 M ammonium sulfate, 1 mM $CoCl_2$, and 0.1 mM $Hg(CH_3COO)_2$ for 60 h or 0.1 mM ethylmercury thiosalicylate (EMTS) for 12 h. [b] $R_{sym} = \sum_{hkl}\sum_i|I(hkl)_i - \langle I(hkl)\rangle|/\sum_{hkl}\sum_i I(hkl)_i$. [c] $R_{iso} = \sum_{hkl}|F_{PH}(hkl) - F_P(hkl)|/\sum_{hkl}F_P(hkl)$. [d] $R_c = \sum_{hkl}||F_{PH}(hkl)| \pm |F_P(hkl)|| - |F_{Hcalc}(hkl)||/\sum_{hkl}||F_{PH}(hkl)| \pm |F_P(hkl)||$ for centric reflections.

association" of the subunits, which allows free access of the substrate to the active sites at the outer faces of the double barrel structure, seems to be the main stabilizing factor in tPRAI.

MATERIALS AND METHODS

Crystallization and Data Collection. Crystals that were grown as described (Sterner et al., 1996) belong to the hexagonal space group $P6_122$ with cell dimensions $a = b = 68.4$ Å, $c = 185.4$ Å, $\alpha = \beta = 90°$, and $\gamma = 120°$. The crystals were mounted in glass capillaries and analyzed using a MAR-Research imaging plate area detector mounted on an Elliott GX-20 rotating anode generator (Cu Kα, 40 kV and 50 mA). They diffract to better than 1.7 Å resolution, but because of 0.45° mosaicity of the crystals and the relatively long *c*-axis, data were collected to only 2.0 Å. For complete native data collection two data sets were measured using crystal to image plate distances of 140 and 220 mm and overall rotation angles of 53° and 31°, respectively (Table 1). For each derivative data collection one data set using a 240 mm crystal to image plate distance and a 45° overall rotation was measured. A rotation angle of 0.3° was used for each exposure to reduce overlapping reflections.

Data were evaluated with the MOSFLM program package (CCP4, 1994). The integrated intensities were scaled with the program ROTAVATA and merged using AGROVATA. The reflection intensities were finally converted to structure factor amplitudes using TRUNCATE (CCP4, 1994). Details on data collection parameters and statistics of the measured data are summarized in Table 1.

Phase Determination. The structure of tPRAI was determined using the method of multiple isomorphous replacement (MIR). The locations of the heavy atom sites were determined by difference Patterson synthesis for the derivative with $Hg(CH_3COO)_2$ and difference Fourier methods for the EMTS derivative. All calculations were performed using the CCP4 package (CCP4, 1994). The heavy atom parameter refinement with MLPHARE resulted in a major site (Cys7) and a minor site (Cys91) for Hg^{2+} and the same sites with about equal occupancy for the EMTS derivative. Phase calculation resulted in an overall figure of merit of 0.40 for data in the range of 10.0−2.8 Å resolution. Combined solvent flattening and histogram matching as implemented in DM (CCP4, 1994) were used to improve the phases. The resulting electron density map, calculated at 2.8 Å resolution, was of sufficient quality to trace 80% of the polypeptide chain.

Model Building and Refinement. An atomic model was built from the "bones" coordinates with the graphics package O (Jones et al., 1991). The atomic model was refined using the X-PLOR package (Brünger, 1992) with the atomic restraint parameters of Engh and Huber (1991) as well as restraints in standard deviations for temperature factor refinement of 2.0/3.0 and 3.0/6.0 for main chain and side chain atoms connected by a bond/angle, respectively.

Table 2: Refinement Statistics

no. of protein atoms	1561
no. of water molecules	106
no. of phosphate (sulfate) molecules	1
rms distances (1−2) (Å)	0.011
rms bond angles (deg)	2.4
R-factor (10.0−2.0 Å, no σ cutoff)	0.192
free *R*-factor (10.0−2.0 Å, 5% data)	0.243
av *B*-factor for protein atoms (Å^2)	32.1
av *B*-factor for water molecules (Å^2)	45.2
av *B*-factor for phosphate (sulfate) molecule (Å^2)	47.3
SD of the real space correlation coeff	0.07
av of the real space correlation coeff	0.93

Initially, the model was subjected to a full simulated annealing refinement procedure using data between 10.0 and 2.8 Å. This reduced the *R*-factor from 46.1% to 24.4% (free *R*-factor for 5% of the data 33.7%) for data between 10.0 and 2.8 Å resolution. Further cycles of manual rebuilding as well as refinement of coordinate and temperature factors were performed, during which water molecules were also built into the structure. The current model includes the polypeptide chain from the N-terminal residue Met1 to the C-terminal residue Leu205. The conformation of the loop containing the residues Thr129−Lys137 could not be identified because of poor electron density, and this loop was excluded from refinement. This model finally gave an *R*-factor of 19.2% for the working data and 24.3% for the test data (free *R*-factor, no σ cutoff) in the resolution range 15.0−2.0 Å and has good stereochemistry (Table 2).

RESULTS AND DISCUSSION

Overall Fold and Secondary Structure. tPRAI is a homodimer in solution under a wide range of conditions (Sterner et al., 1996). tPRAI crystallizes accordingly as an α_2 dimer, with the molecular 2-fold axis coinciding with the crystallographic 2-fold axis. As a consequence, the asymmetric unit comprises one subunit of the dimer. The structural model of this subunit contains 196 (of the total of 205) amino acid residues, 106 ordered water molecules, and a phosphate (or sulfate, cf. below) ion. According to the Ramachandran plot for tPRAI (not shown) 92.9% of the non-glycine residues lie in the most favored and 7.1% in the additionally allowed regions, respectively. No non-glycine residue is in the disallowed regions. The subunits of tPRAI consist of a single domain with the $(\beta\alpha)_8$- or triose phosphate isomerase (TIM)-barrel fold (Banner et al., 1975). Figure 1 gives an overview of the folding topology of dimeric tPRAI. The axes of the two parallel β-barrels are almost parallel and about 14 Å apart. The monomers of tPRAI interact through the N-terminal faces of their β-barrels. The active

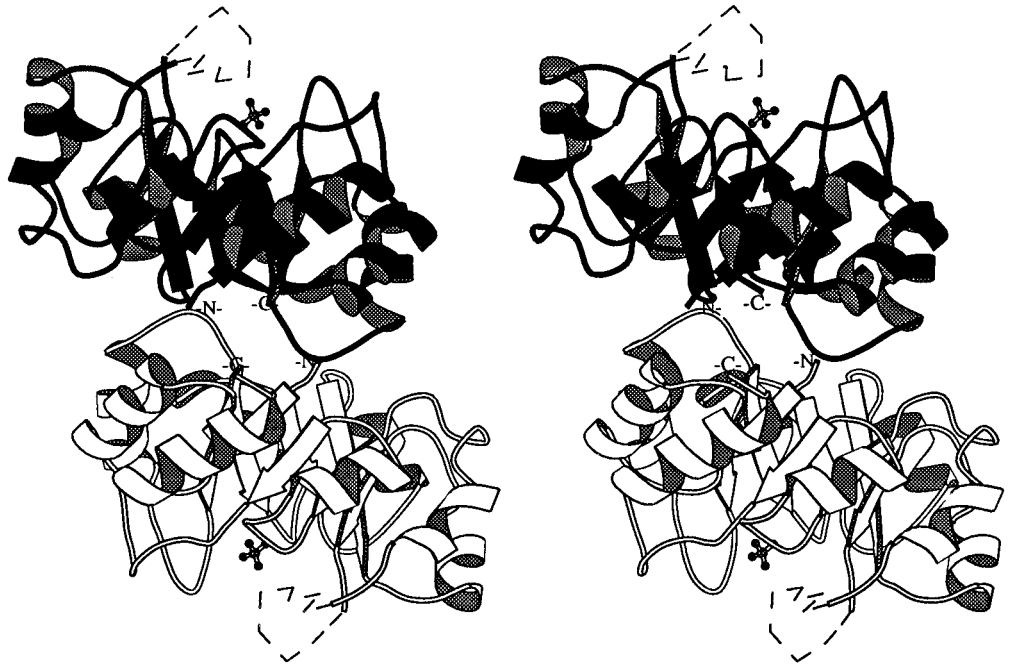

FIGURE 1: tPRAI is a dimer of two identical $(\beta\alpha)_8$-barrel subunits. The ribbon diagram shows that the subunits associate via the N-terminal faces of their β-barrels. The active sites, identified by the bound phosphate/sulfate ion, are at opposite sides of the dimer, most distant from the dimer interface. The loop connecting strand β6 with helix α6, which is not visible in the electron density, is drawn as a dashed line.

```
          β1          α1          β2                    α2          β3          α3          β4          α4          β5
          SSSS      HHHHHHHHHH    SSSSS               HHHHHHHHHH    SSSSSS    HHHHHHHHHH    SSSS      HHHHHHH     SSSSSSSS
        1        10          20          30          40          50          60          70          80          90          100
tPRAI   MVRVKICGITNLEDALFSVESGADAVGFVFYPKSKRYISPEDARRISVELPPFVFRVGVFVNEEPEKILDVASYVQLNAVQLHGEEPIELCRKIAER----ILVIKAVGVS
            § §§ |   ||        ||   §  |   | |     | |                 |||| |        | |     | ||§|§| |          |          ||  |
ePRAI     ENKVCGLTRGQDAKAAYDAGAIYGGLIFVATSPRCVNVEQAQEVMAAA--PLQYVGVFRNHDIADVVDKAKVLSLVAVQLHGNEEQLYIDTLREALPAHVAIWKALSVG
             260         270         280         290         300         310         320         330         340         350         360
          SSSS      HHHHHHHHHH    SSSSS               HHHHHHHH      SSSSSS    HHHHHHHHHH    SSSS      HHHHHHHHHH    SSSSSSS
          β1          α1          β2                    α2          β3          α3          β4          α4          β5
```

```
          α5          β6                    α6          β7          α7       β8  α8′          α8
         HHHHHHH      SSSSS               HHHHHHHHHH   SSSS      HHHHHHHH   SSSS HHH      HHHHHHHHHHHH
          110       120         130       140         150         160         170       180       190       200
tPRAI   NERDMERALNYREF-PILLDTKTPEYGGSGKTFDWSLILPYRDRFRYLVLSGGLNPENVRSAIDVVRPFAVDVSSGVEAFPGKKDHDSIKMFIKNAKGL
              |          |§       |§|§  |||||           | §§|    |    |          §  | |§   |§ ||
ePRAI   ---ETLPAREFQHVDKYVLDNGQ---GGSGQRFDWSLLNGQSL--GNVLLAGGLGADNCVEAAQTG-CAGLDFNSAVESQPGIKDARLLASVFQTLRAY
             370         380         390         400         410         420         430       440       450
                    SSSSS               HHHH        SSS         HHHHH      SSSS HHH      HHHHHHHHHHHH
                     β6                  α6          β7          α7         β8  α8′          α8
```

FIGURE 2: Sequence alignment and position of the secondary structural elements in both tPRAI and ePRAI. The alignment of the amino acid sequences [Christie and Platt (1980) for ePRAI; Sterner et al. (1995) for tPRAI] is based on the superposition of the three-dimensional structures (cf. Figure 3) of tPRAI and ePRAI (Wilmanns et al., 1992). The single-letter code for amino acid residues is used. The numbering scheme and the position and assignment of the secondary structural elements are shown above and below the sequences for tPRAI and ePRAI, respectively. Identical residues (30%) between tPRAI and ePRAI are indicated by (|), and invariant residues for PRAI from 19 sequences in the SWISSPROT data bank (Sterner et al., 1995) are marked by (§).

sites, which are identified by the bound phosphate/sulfate ion, lie on opposite faces of the dimer. All nine residues of the polypeptide chain that were not visible in the electron density (Thr129−Lys137) belong to the disordered loop that connects strand β6 and helix α6. Loop β6α6, which is also disordered in ePRAI (Priestle et al., 1987; Wilmanns et al., 1992), contains two invariant glycine residues (Figure 2) that may play an important functional role (Luger et al., 1989).

Superposition of the backbone structures of tPRAI and its thermolabile counterpart ePRAI shows that the two enzymes share a very similar overall fold (Figure 3) with a root mean square deviation of 1.4 Å for 178 Cα positions. Nevertheless, the secondary structural elements (as defined by DSSP; Kabsch et al., 1983) of tPRAI and ePRAI show several differences. Helix α5 of tPRAI that includes residues Glu109−Ala115, is absent in the structure of ePRAI, where the corresponding segment is rigid but does not have a defined secondary structure (Figures 3 and 4). Seventy-five residues of tPRAI are involved in helical structure (corresponding to 37% of all residues) as compared to 63 residues (32%) in ePRAI. No uniform picture emerges when the potential stabilities of α-helices in tPRAI and ePRAI are compared. The content of alanine residues within α-helices, which has been correlated with thermostability (Menendez-Arias & Argos, 1989), is higher in ePRAI (13 alanines out of 63 α-helical residues) than in tPRAI (6 alanines out of 75 α-helical residues). α-Helices can also be stabilized by compensating the positive and negative poles of their macrodipoles (Chakrabartty & Baldwin, 1995) through negatively charged residues in the first and positively charged residues in the last helical turn. Judged by this criterion, α-helices of tPRAI (eight negatively and four positively charged residues) would be slightly more stable than α-helices of ePRAI (four negatively and three positively

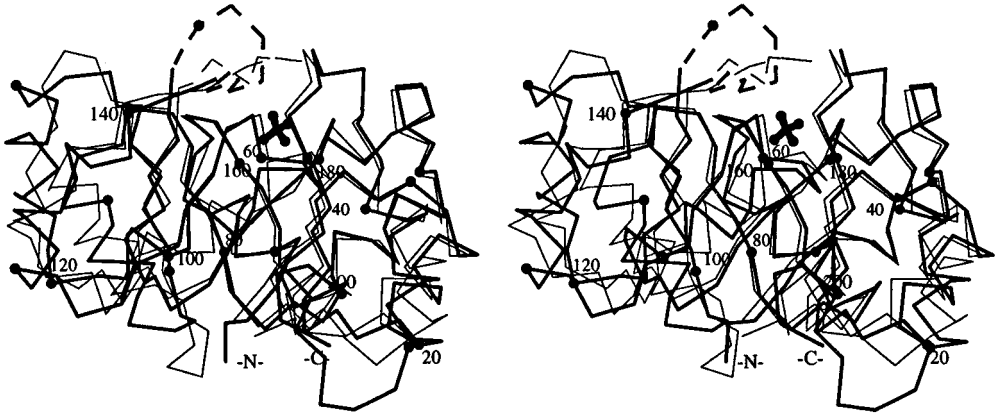

FIGURE 3: Superimposed Cα traces of one subunit of tPRAI (thick lines) and ePRAI (artificially separated from the eIGPS domain, thin lines). The N- and C-termini of the polypeptide chain are marked for tPRAI, as well as every 20th amino acid residue (by a dot). The active site is identified by the bound phosphate/sulfate ion. The most striking difference between tPRAI and ePRAI is the loop connecting helix α2 with strand β3, which is longer in tPRAI (residues Pro51−Val54).

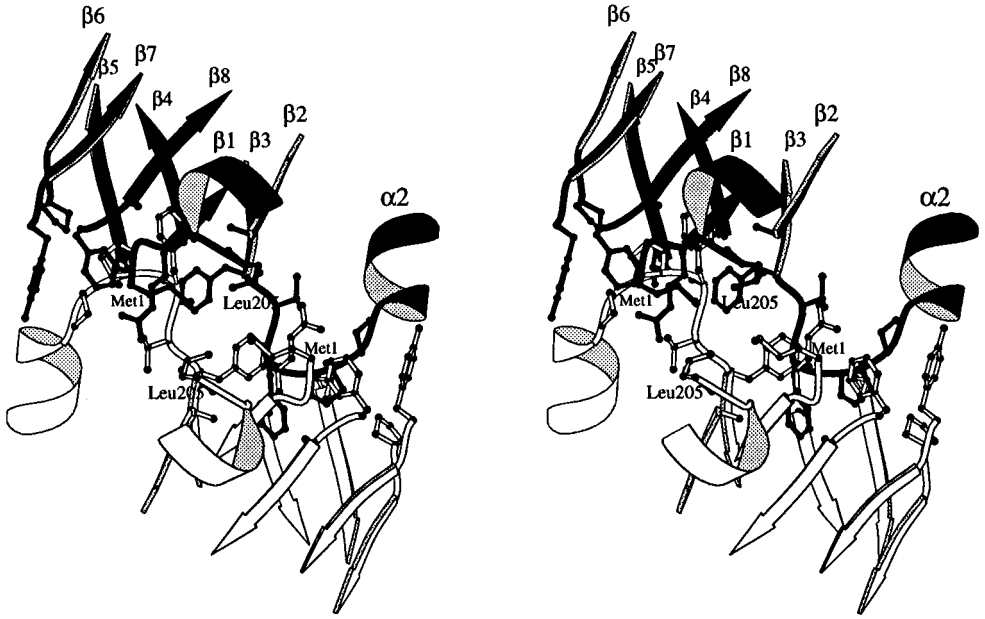

FIGURE 4: The subunits of the tPRAI dimer are associated via strong hydrophobic contacts. The hydrophobic residues of the loop that connects helix α2 with strand β3 (Pro51-Pro52-Phe53-Val54) protrude into the interior of the β-barrel of the other subunit. Due to the 2-fold symmetry of tPRAI, this contact is formed twice. The N-terminal and C-terminal residues of both subunits, Met1 and Leu205, form a hydrophobic cluster at the dimer interface.

charged residues, Figure 2). The fractions of residues involved in β-sheet structures in tPRAI (40 residues, corresponding to 20%) and ePRAI (38 residues, corresponding to 19%) are almost identical. The lengths of the loops connecting α-helices with β-strands at the N-terminal side of the barrel are quite different for the two enzymes (Figure 2). This feature reflects in part the "engineering" of the dimer interface in tPRAI.

Comparison of the amino acid composition of the two enzymes shows that the number of prolines is increased from 5 residues in ePRAI to 11 residues in tPRAI. Most of the additional prolines in the thermostable protein are either in loops or initiate α-helices. The number of glycine residues is reduced from 20 in ePRAI to 11 in tPRAI. Both the increase of the number of prolines and the reduction of the number of glycines must reduce the entropy of the unfolded state and consequently stabilize tPRAI (Watanabe et al., 1991).

Dimer Interface. Fifteen percent (1450 Å^2, program DSSP; Kabsch et al., 1983) of the total solvent-accessible surface area of each subunit is buried in tPRAI. The two loops α2β3 provide for an unusual mode of interlocking interaction that is likely responsible for the stability of the dimer (Figure 4). The sequence of hydrophobic residues (Pro51-Pro52-Phe53-Val54) residing in loops α2β3 protrudes reciprocally into the interior of the β-barrel of the neighboring subunit and is completely inaccessible to solvent. As a result, Pro52 of one subunit fits into the bottom (0) layer of the barrel (Wilmanns et al., 1992) of the other subunit, which is formed by the side chains of Arg3′ (strand β1), Phe55′ (strand β3), Leu99′ (strand β5), Tyr 153′ (strand β7), and Phe175′ (strand β8). In addition, Phe53 fits into the first regular layer (1) of the barrel, which consists of Ala25′ (strand β2), Ala79′ (strand β4), Pro122′ (strand β6), and Ala 176′ (strand β8).

This highly stabilizing intersubunit interaction occurs twice, due to the 2-fold symmetry of tPRAI (Figure 4). When all 19 PRAI sequences collected in the SWISSPROT databank are aligned (Sterner et al., 1995), we find that only the PRAI from the halophilic archaeon *Haloferax volcanii* has a similarily long and hydrophobic amino acid sequence

Table 3: Comparison of Salt Bridges in tPRAI and ePRAI[a]

positively charged side chain	mean *B*-factor[b] (Å^2)	ACC[c] (Å^2)	position	negatively charged side chain	mean *B*-factor[b] (Å^2)	ACC[c] (Å^2)	position	distance (Å)
tPRAI								
Lys5 Nζ	25.5	0	β1	Asp178 Oδ1	28.2	8	β8	2.79
Arg36 Nη1	53.3	44	β2−α2	Glu184 Oε1	30.6	31	β8−α8	2.72
Arg36 Nη1	53.3	44	β2−α2	Glu184 Oε2	30.6	31	β8−α8	2.93
Arg45 Nη1	55.5	167	α2	Asp42 Oδ2	41.1	21	α2	3.09
Lys67 Nζ	56.6	85	α3	Glu63 Oε2	37.6	36	β3−α3	3.42
Lys67 Nζ	56.6	85	α3	Glu63 Oε1	37.6	36	β3−α3	3.42
His83 Nε2	28.8	48	β4−α4	Asp126 O2	31.0	12	β6	3.07
Arg92 Nη1	42.7	117	α4	Glu120 Oε1	42.8	88	α5−β6	2.71
Arg92 Nη1	42.7	117	α4	Glu120 Oε2	42.8	88	α5−β6	3.34
Lys93 Nζ	55.4	89	α4	Glu96 Oε1	58.3	105	α4−β5	3.51
Lys102 Nζ	26.6	0	β5	Glu86 Oε1	25.1	1	β4−α4	3.09
Arg148 Nη2	38.2	91	α6	Asp149 Oδ1	35.2	131	α6	2.65
Arg152 Nη2	68.3	105	α6−β7	Glu49[d] Oε2	47.7	66	α2	2.76
Arg173 Nη1	63.5	125	α7−β8	Asp170 Oδ1	62.7	82	α7	3.26
Lys189 Nζ	24.8	70	β8−α8	Asp14 Oδ1	25.6	1	α1	3.05
His192 Nε2	26.7	61	α8	Asp14 Oδ1	25.6	1	α1	2.84
Lys196 Nζ	27.3	93	α8	Asp193 Oδ1	36.8	93	α8	3.22
Lys203 Nζ	26.1	41	α8	Asp24 Oδ1	26.1	6	α1−β2	3.31
Lys203 Nζ	26.1	41	α8	Asp24 Oδ2	26.1	6	α1−β2	2.96
ePRAI								
Lys258 Nζ	11.9	0	β1	Asp425 Oδ2	26.3	14	β8	2.62
Arg264 Nη1	44.2	77	β1−α1	Asp267 Oδ1	24.9	129	α1	2.70
Arg264 Nη1	44.2	77	β1−α1	Asp267 Oδ2	24.9	129	α1	3.23
Lys269 Nζ	56.0	87	β1	Asp273Oδ1	21.9	92	α1	2.83
Arg289 Nη1	35.7	13	β2−α2	Glu431 Oε1	26.5	26	β8−α8	2.31
Arg289 Nη1	35.7	13	β2−α2	Glu431 Oε2	26.5	26	β8−α8	3.48
His314 Nε2	17.9	45	β3−α3	Asp318 Oδ2	18.4	68	α3	2.65
Lys322 Nζ	24.7	31	α3	Asp318Oδ2	18.4	68	α3	3.17
Lys322 Nζ	24.7	31	α3	Asp318Oδ1	18.4	68	α3	3.20
Lys357 Nζ	27.8	6	β5	Glu337Oε1	16.6	5	β4α4	3.34
His372 Nε2	36.6	84	β5−β6	Asp343 Oδ1	24.9	40	α4	3.48
Lys437 Nζ	25.0	5	β8α8	Glu431Oε2	26.5	26	β8α8	2.55

[a] All salt bridges with distances less than 3.7 Å between the nitrogen and the nearest oxygen atom are included. The assignment of residues to secondary structural elements is documented in Figure 2. With one exception, all salt bridges of tPRAI are intrasubunit. [b] Mean *B*-factor for side chain; average *B*-factor for all side chain atoms in tPRAI is 32.4 Å^2. [c] Solvent-accessible surface of the residue. [d] Residue from the second subunit of the dimer.

as tPRAI between helix α2 and strand β3, namely, Ala-Pro-Pro-Phe-Leu (Lam et al., 1992). This observation suggests that also this "extremophilic" PRAI is stabilized by dimerization via contacts at the N-terminus of the β-barrels. The N- and C-termini of the two polypeptide chains are also part of the dimer interface of tPRAI (Figures 1 and 4). The side chains of Met1 and Leu205 form an hydrophobic cluster close to the surface of the molecule but shielded from the solvent by polar main chain atoms. The positive and the negative charges of the termini point into the solvent. Thus, the termini of the polypeptide chain mutually prevent each other from "fraying".

In another thermostable TIM-barrel protein, indole-3-glycerol phosphate synthase from *Sulfolobus solfataricus*, the stabilization of the termini is achieved by a different mechanism, namely, by salt bridges between the N-terminal ammonium group and a glutamate and between the C-terminal carboxylate group and an arginine side chain (Hennig et al., 1995). Intermolecular hydrogen bonds of tPRAI include the salt bridge between Glu49 (helix α2) and Arg152′ (loop α6β7). However, the rather high *B*-factors indicate flexibility of these side chains and consequently only a weak interaction (Table 3). In addition, the side chain of Arg3 (strand β1) forms hydrogen bonds to the main chain carbonyl oxygen atoms of Val19′ (helix α1) and of Ala23′ (loop α1β2). Disregarding water-mediated hydrogen bonds, polar interactions between the subunits are rare.

The mode of dimerization of the subunits of tPRAI is quite different from what has been observed for other TIM-barrel proteins. In homodimeric TIM, the barrel axes are in a similar direction and the subunits associate sideways, mainly via helices α2 and α3 as well as via loops β2α2, β3α3, and β4α4 (Wierenga et al., 1992). In the homodimeric dihydropteroate synthase, a sideways association also occurs via helices α7′, α7, and α8, but the barrel axes have opposite directions (Hampele et al., 1997).

In the bifunctional enzyme eIGPS:ePRAI the interface is formed by residues of both domains that are located mainly in α-helices and in loops on both sides of the barrels (Wilmanns et al., 1992). The interdomain surface area in eIGPS:ePRAI is 810 Å^2, only about half the interface area of tPRAI.

Dimer formation in tPRAI via strong hydrophobic interactions might contribute in several ways to its extreme thermostability, judged by its half-life for inactivation of 310 min at 85 °C (Sterner et al., 1996). First, the tight association with a intersubunit surface area of 1450 Å^2 minimizes the accessible surface to volume ratio by 13% (0.219 vs 0.248 for the monomeric tPRAI), a feature that has been related to thermostability in the dimeric aldehyde ferredoxin reductase from *Pyrococcus furiosus* (Chan et al., 1995). However, also in the bifunctional enzyme eIGPS:PRAI, the surface to volume ratio is decreased by 11% compared to the isolated ePRAI domain (0.227 vs 0.252).

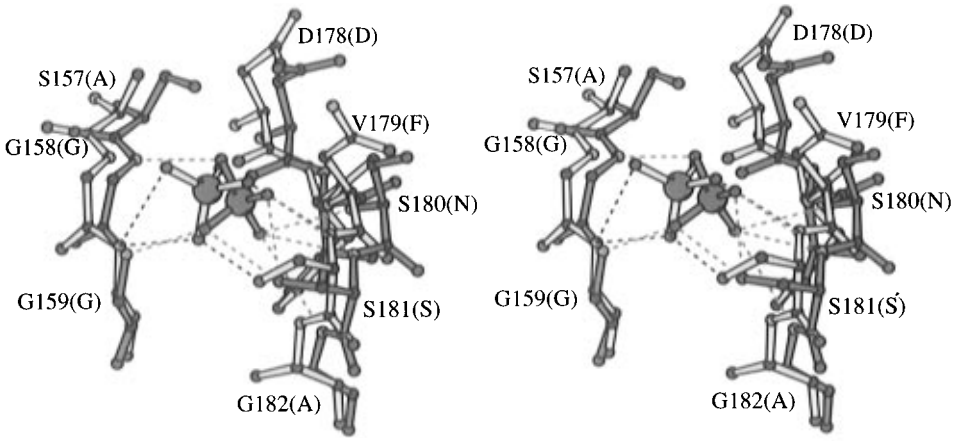

FIGURE 5: Phosphate binding site of PRAIs. tPRAI maintains more hydrogen bonds to the phosphate/sulfate ion than ePRAI. Residue numbers are given for tPRAI (Figure 2); corresponding residues of ePRAI are in brackets. Stick representation of main chains: green, tPRAI; yellow, ePRAI. Ball representation of atoms: black, carbon; red, oxygen; blue, nitrogen; purple, phosphorus/sulfur. Hydrogen bonds, dashed lines: green, tPRAI; black, ePRAI. The phosphate oxygen atoms are denoted PO1, PO2, PO3, and PO4. Lengths between hydrogen bond donors and acceptors for ePRAI are PO1−Gly407(N) 2.79 Å, PO1−Ser428(Oγ) 3.26 Å, PO2−Ser428(N) 3.03 Å, and PO4−Gly407(N) 3.58 Å and for tPRAI are PO1−Ser180(N) 2.99 Å, PO1−Ser181(N) 3.57 Å, PO1−Gly182(N) 3.70 Å, PO2−Gly158(N) 3.59 Å, PO3−Gly159(N) 3.01 Å, PO3−Ser181(Oγ) 3.49 Å, PO4−Ser181(N) 3.23 Å, and PO4−Ser181(Oγ) 3.01 Å (program MOLSCRIPT; Kraulis, 1991).

Second, strong hydrophobic interactions at the dimer interface have been shown by site-directed mutagenesis to be important determinants of thermostability of dimeric 3-isopropylmalate dehydrogenases from *Thermus thermophilus* (Kirino et al., 1994). Also, a structural comparison showed that the hydrophobic interactions at the dimer interface were more pronounced in TIM from the thermophile *Bacillus stearothermophilus* than in TIMs from five different mesophilic species (Delboni et al., 1995).

Dimer formation (and thus stabilization) of tPRAI appears to be mainly accomplished by the loop $\alpha 2\beta 3$ (Figure 4). This finding is in accordance with earlier studies on PRAI from yeast (Luger et al., 1989) and ePRAI (Urfer & Kirschner, 1992), which showed that loops at the N-terminal face of the β-barrel (loops $\alpha_i\beta_{i+1}$) are important determinants of the stability of these TIM-barrel proteins. Since residues of tPRAI involved in catalysis are located in loops at the C-terminal face of the barrel (loops $\beta_i\alpha_i$), the concept of divided labor between loops $\beta_i\alpha_i$ (catalysis) and loops $\alpha_i\beta_{i+1}$ (stability) in $(\beta\alpha)_8$-barrels is supported by the mode of dimerization of the subunits of tPRAI.

Phosphate Ion Binding Site. Electron density indicative of a phosphate ion signals the potential binding site of the phosphate−ester moiety of the substrate phosphoribosyl anthranilate (Wilmanns et al., 1992) in ePRAI. Electron density was also detected at the equivalent position in tPRAI (Figures 2 and 4). However, since 1.5 M ammonium sulfate was used as precipitant for crystallization (Sterner et al., 1996), it cannot be excluded that the active sites have bound sulfate ions, as discussed for the related $(\beta\alpha)_8$-barrel enzymes IGPS from *E. coli* and *S. solfataricus* (Hennig et al., 1995; Knöchel et al., 1996). In the known structures of IGPS the phosphate/sulfate ion is bound at the N-terminal turn of the additional α-helix α8′ that is located in the loop between strand β8 and helix α8 (Wilmanns et al., 1992; Hennig et al., 1995; Knöchel et al., 1996). Superposition of the two structures reveals almost identical locations but different orientations of the phosphate ion (Figure 5). This observation is puzzling because of the rather similar conformation of the two binding sites. The only difference is the more bulky side chains for residues N427 and A429 in ePRAI compared to S181 and G182 in tPRAI that cause a better fit of the helix α8′ to the phosphate ion in the thermostable structure.

Helix α8′ is also present in the structures of tPRAI (and ePRAI) (Figure 2), but it is shorter and less ordered than in the known IGPS structures, as indicated by the ϕ,ψ angles for Ser181 (−74°, −21°), Gly182 (−67°, −10°), and Glu184 (−130°, 25°). The phosphate binding site consists of residues of helix α8′ and of the neighboring loop β7α7 (Figure 5): Using a distance cutoff of 3.7 Å, there are eight hydrogen bonds to oxygen atoms of the phosphate/sulfate ion in tPRAI. They are maintained by peptide amide groups of the invariant residues Gly 158, Gly159 (loop β7α7), Ser 180, Ser181, and Gly182 (helix α8′), as well as by the side chain of Ser181. Only four stable hydrogen bonds to oxygen atoms of the phosphate/sulfate exist in ePRAI. They involve the peptide amide of Gly407 (corresponding to Gly159 in tPRAI; Figure 2), as well as the peptide amide and the side chain of Ser428 (corresponding to Ser181 in tPRAI). The location and distances of the hydrogen bonds are given in Figure 5.

Salt Bridges. Several recent publications on highly resolved crystal structures of thermophilic enzymes focus on the role of ionic interactions in protein stabilization (Davies et al., 1993; Kelly et al., 1993; Korndörfer et al., 1995; Yip et al., 1995). In particular, indole-3-glycerol phosphate synthase from the hyperthermophile *S. solfataricus* (sIGPS) contains 24 salt bridges, compared to only 11 salt bridges of the thermolabile eIGPS (Hennig et al., 1995; Knöchel et al., 1996).

Table 3 presents all salt bridges in tPRAI and ePRAI, defined as ion pairs with a distance of less than 3.7 Å between the hydrogen-bonded oxygen and nitrogen atoms (Barlow & Thornton, 1983). The average temperature factors and solvent accessibilities of the involved residues are listed to better evaluate the relative strengths of the individual salt bridges. tPRAI has a total of 15 salt bridges per subunit, whereas ePRAI has only 9. Three salt bridges that are close to the active site are conserved between the two structures

(Lys5/Asp178, Arg36/Glu184, and Lys102/Glu86 in tPRAI). A remarkable difference is that five salt bridges in tPRAI are formed between residues of α-helices and loops $\alpha_i\beta_{i+1}$, whereas in ePRAI three salt bridges are formed at the opposite face of the central β-barrel, that is, between residues of loops $\beta_i\alpha_i$. Another significant difference is observed in the number of salt bridges between residues that are far apart in the sequence (eight in tPRAI and one in ePRAI; cf. Table 3). In contrast to sIGPS (Hennig et al., 1995), tPRAI neither shows salt bridge clusters nor does it contain a great number of ion pairs that clamp adjacent α-helices. Thus, in accordance with the previous findings on the role of salt bridges in thermostable proteins, tPRAI has a greater number of ion pairs than ePRAI, but their effect on stability seems to be less important than in sIGPS.

Conclusions. The comparison of the crystal structures of the extremely thermostable enzyme phosphoribosyl anthranilate isomerase from *T. maritima* and its thermolabile counterpart from *E. coli* shows distinct differences that are likely responsible for their different stabilities. Most strikingly, tPRAI is a homodimer, the subunits of which associate via the bottoms of their β-barrels involving strong hydrophobic contacts. In contrast, ePRAI is part of a bifunctional enzyme. Thus, the structure of tPRAI carries the concept of divided labor between loops located on the two ends of $(\alpha\beta)_8$-barrels to the extreme: Whereas loops at the top of the barrel provide for catalytic residues and therefore are important for catalytic function, loops at the bottom of the barrel contribute strongly to stability (Luger et al., 1989; Urfer & Kirschner, 1992). Other potentially stabilizing features of tPRAI are the mutual immobilization of the chain termini (Met1 and Leu205) by hydrophobic interactions and the articulation of helix α5, which is only a loop in ePRAI. Furthermore, as manifested in the TIM-barrel domain of a thermostable glucosidase (Watanabe et al., 1991), a decrease of entropy of the unfolded state by an increased number of prolines located in loops may contribute to the thermostability of tPRAI. The number of salt bridges in tPRAI is increased compared to ePRAI. However, compared to another hyperthermostable TIM-barrel enzyme of tryptophan biosynthesis, indole-3-glycerol phosphate synthase from *S. solfataricus* (Hennig et al., 1995), stabilization by salt bridges is not dominant in tPRAI. Thus, different mechanisms of stabilization toward thermal denaturation are found even in structurally closely related enzymes.

Due to an improved substrate affinity (at 25 °C, K_M^{PRA} values are 0.28 and 12.2 μM for tPRAI and ePRAI, respectively) the catalytic efficiency (k_{cat}/K_M^{PRA}) of tPRAI is 5-fold greater than that of ePRAI, even at 25 °C (Sterner et al., 1996). This observation is unusual, because many enzymes from hyperthermophilic organisms are almost inactive at room temperature (Jaenicke et al., 1996). Comparison of the phosphate binding sites, which are part of the substrate binding sites, identifies a greater number of hydrogen bonds to the phosphate ion in tPRAI than to the phosphate ion in ePRAI. Therefore, the differences in phosphate binding may be responsible for the greater catalytic efficiency of tPRAI which is necessary to outrun the spontaneous hydrolysis of the thermolabile substrate PRA, particularly at 80 °C, the optimal growth temperature of *T. maritima*.

ACKNOWLEDGMENT

We thank Halina Szadkowski for dedicated assistance and Dr. Gerd Kleemann for critical discussions.

REFERENCES

Adams, M. W. W. (1993) *Annu. Rev. Microbiol. 47*, 627−658.
Banner, D. W., Bloomer, A. C., Petsko, D. C., Phillips, D. C., Pogson, C. I., Wilson, I. A., Corran, P. H., Furth, A. J., Milman, R. J., Offord, R. E., Priddle, J. D., & Waley, S. G. (1975) *Nature 255*, 609−614.
Barlow, D. J., & Thornton, J. M. (1983) *J. Mol. Biol. 168*, 867−885.
Brünger, A. T. (1992) *X-PLOR Version 3.1. A System for X-ray Crystallography and NMR*, Yale University Press, New Haven and London.
Chakrabartty, A., & Baldwin, R. L. (1995) *Adv. Protein Chem. 46*, 141−173.
Chan, M. K., Mukund, S., Kletzin, A., Adams, M. W. W., & Rees, D. C. (1995) *Science 267*, 1463−1469.
Christie, G. E., & Platt, T. (1980) *J. Mol. Biol. 142*, 519−530.
Collaborative Computational Project, Number 4 (1994) The CCP4 suite: programs for protein crystallography, *Acta Crystallogr. D50*, 760−763.
Creighton, T. E. (1970) *Biochem. J. 120*, 699−707.
Davies, G. J., Gamblin, S. J., Littlechild, J. A., & Watson, H. C. (1993) *Proteins: Struct., Funct., Genet. 15*, 283−289.
Day, M. W., Hsu, B. T., Joshua-Tor, L., Park, J.-B., Zhou, Z. H., Adams, M. W. W. & Rees, D. C. (1992) *Protein Sci. 1*, 1494−1507.
Delboni, L. F., Mande, S. C., Rentier-Delrue, F., Mainfroid, V., Turley, S., Vellieux, F. M. D., Martial, J. A., & Hol, W. G. J. (1995) *Protein Sci. 4*, 2594−2604.
Eberhard, M., Tsai-Pflugfelder, M., Bolewska, K., Hommel, U., & Kirschner, K. (1995) *Biochemistry 34*, 5419−5428.
Engh, R. A., & Huber, R. (1991) *Acta Crystallogr. A 47*, 392−400.
Fujinaga, M., Berthet-Colominas, C., Yaremchuk, A. D., Tukalo, M. A., & Cusack, S. (1993) *J. Mol. Biol. 234*, 222−233.
Hampele, I., D'Arcy, A., Dale, G. E., Kostrewa, D., Nielsen, J., Oefner, Ch., Page, M. G. P., Schönfeld, H. J., Stüber, D., & Then, R. L. (1997) *J. Mol. Biol. 268*, 21−30.
Hennig, M., Darimont, B., Sterner, R., Kirschner, K., & Jansonius, J. N. (1995) *Structure 3*, 1295−1306.
Huber, R., Langworthy, T. A., König, H., Thomm, M., Woese, C. R., Sleytr, U. B., & Stetter, K. O. (1986) *Arch. Microbiol. 144*, 324−333.
Imada, K., Sato, M., Tanaka, N., Katsube, Y., Matsuura, Y., & Oshima, T. (1991) *J. Mol. Biol. 222*, 725−738.
Jaenicke, R., Schurig, H., Beaucamp, N., & Ostendorp, R. (1996) *Adv. Protein Chem. 48*, 181−269.
Jones, T. A., Zou, J. Y., Cowan, S. W., & Kjeldgaard, M. (1991) *Acta Crystallogr. A47*, 110−119.
Kabsch, W., & Sander, Ch. (1983) *Biopolymers 22*, 2577−2637.
Kelly, C. A., Nishiyama, M., Ohnishi, Y., Beppu, T., & Birktoft, J. J. (1993) *Biochemistry 32*, 3913−39232.
Kirino, H., Aoki, M., Aoshima, M., Hayashi, Y., Ohba, M., Yamagishi, A., Wakagi, T., & Oshima, T. (1994) *Eur. J. Biochem. 220*, 275−281.
Knegtel, R. M. A., Wind, R. D., Rozeboom, H. J., Kalk, K. H., Buitelaar, R. M., Dijkhuizen, L., & Dijkstra, B. W. (1996) *J. Mol. Biol. 256*, 611−622.
Knöchel, T. R., Hennig, M., Merz, A., Darimont, B., Kirschner, K., & Jansonius, J. N. (1996) *J. Mol. Biol. 262*, 502−515.
Korndörfer, I., Steipe, B., Huber, R., Tomschy, A., & Jaenicke, R. (1995) *J. Mol. Biol. 246*, 511−521.
Kraulis, P. J. (1991) *J. Appl. Crystallogr. 24*, 946−950.
Lam, W. L., Logan, S. M., & Doolittle, W. F. (1992) *J. Bacteriol. 174*, 1694−1697.
Laskowski, R., MacArthur, M., Moss, D., & Thorton, J. (1993) *J. Appl. Crystallogr. 26*, 283−291.
Luger, K., Hommel, U., Herold, M., Hofsteenge, J., & Kirschner, K. (1989) *Science 243*, 206−210.
Macedo-Ribeiro, S., Darimont, B., Sterner, R., & Huber, R. (1996) *Structure 4*, 1291−1301.

Menéndez-Arias, L., & Argos, P. (1989) *J. Mol. Biol. 206*, 397−406.

Priestle, J. P., Grütter, M. G., White, J. L., Vincent, M. G., Kania, M., Wilson, E., Jardetzky, T. S., Kirschner, K., & Jansonius, J. N. (1987) *Proc. Natl. Acad. Sci. U.S.A. 84*, 5690−5694.

Reardon, D., & Farber, G. K. (1995) *FASEB J. 9*, 497−503.

Russell, R. J. M., Hough, D. W., Danson, M. J., & Taylor, G. L. (1994) *Structure 2*, 1157−1167.

Sterner, R., Dahm, A., Darimont, B., Ivens, A., Liebl, W., & Kirschner, K. (1995) *EMBO J. 14*, 4395−4402.

Sterner, R., Kleemann, G. R., Szadkowski, H., Lustig, A., Hennig, M., & Kirschner, K. (1996) *Protein Sci. 5*, 2000−2008.

Stetter, K. O., Fiala, G., Huber, G., Huber, R., & Segerer, A. (1990) *FEMS Microbiol. Rev. 75*, 117−124.

Tanner, J. J., Hecht, R. M., & Krause, K. L. (1996) *Biochemistry 35*, 2597−2609.

Urfer, R., & Kirschner, K. (1992) *Protein Sci. 1*, 31−45.

Watanabe, K., Chishiro, K., Kitamura, K., & Suzuki, Y. (1991) *J. Biol. Chem. 266*, 24287−24294.

Wierenga, R. K., Noble, M. E. M., & Davenport, R. C. (1992) *J. Mol. Biol. 224*, 1115−1126.

Wilmanns, M., Hyde, C. C., Davies, D. R., Kirschner, K., & Jansonius, J. N. (1991) *Biochemistry 30*, 9161−9169.

Wilmanns, M., Priestle, J. P., Niermann, T., & Jansonius, J. N. (1992) *J. Mol. Biol. 223*, 477−507.

Yip, K. S. P., Stillman, T. J., Britton, K. L., Artymiuk, P. J., Baker, P. J., Sedelnikova, S. E., Engel, P. C., Pasquo, A., Chiaraluce, R., Consalvi, V., Scandurra, R., & Rice, D. W. (1995) *Structure 3*, 1147−1158.

BI962718Q